PadéFroissart exact signal-noise separation in nuclear magnetic resonance spectroscopy

Dževad Belkić, Karen Belkić

Padé-Froissart Exact Signal-Noise Separation in Nuclear Magnetic Resonance Spectroscopy

Dževad Belkić and Karen Belkić

Karolinska Institute, P.O. Box 260, S-171 76 Stockholm, Sweden

Abstract:

Nuclear magnetic resonance spectroscopy is one of the key methods for studying the structure of matter on vastly different levels (sub-nuclear, nuclear, atomic, molecular, cellular, etc). Its overall success critically depends upon reliable mathematical analysis and interpretation of the studied data. This is especially aided by parametric signal processing with the ensuing data quantification, which can yield the abundance or concentrations of the constituents in the examined matter. Such reconstructed information for the most relevant constituents is one of the prerequisites for an accurate assessment of the overall function of the investigated substance.

The sought reliability of signal processing rests upon the possibility of the solution of the quantification problem as well as on the separation of true from false information in the spectrally analyzed data. We presently demonstrate that the diagonal fast Padé transform, as a ratio of two polynomials P_K/Q_K of the common degree K, can yield exact quantification and exact signal-noise separation for noise-free and noise corrupted time signals built from 25 molecules.

Spurious (noise or noise-like) resonances appear in every parametric estimator. The fast Padé transform makes use of pole-zero cancellations via Froissart doublets in the response function P_K/Q_K to unequivocally distinguish genuine (physical) from spurious (unphysical) resonances. Once identified, unphysical resonances are discarded from the final output of the data analysis. Invariably, the number of spurious resonances is by orders of magnitude larger than that of the true ones. The computation is carried out by gradually and systematically increasing the degree K of the Padé polynomials P_K and Q_K. As this degree K changes, the reconstructed parameters and spectra fluctuate until stabilization occurs. The polynomial degree K at which the full stabilization is achieved represents the sought exact number of resonances. An illustrative set of results is reported in this work to show an unequivocal separation of genuine from spurious information by using the denoising Froissart filter. The fast Padé transform for optimal quantification of the physical constituents of the studied matter and the accompanying Froissart filter for unambiguous signal-noise separation is expected to significantly aid nuclear magnetic resonance spectroscopy in achieving the most reliable data analysis and interpretation.

1 Introduction

Nuclear magnetic resonance (NMR) spectroscopy, which is known as magnetic resonance spectroscopy (MRS) in medicine, is one of the most powerful strategies for structural studies of matter on widely different levels and complexities [1]–[5]. Being most thoroughly tested for benchmarking in structural physics, chemistry and biology through multifaceted investigations, including protein structure [6], NMR spectroscopy also became vital in life sciences, particularly in medicine when used for early cancer diagnostics [5]. For example, in oncology, MRS can successfully focus on spectroscopy of molecules (metabolites) of human tissue through timely detection of malignant changes in cells prior to the appearance of the corresponding alterations on anatomical/morphological magnetic resonance images (MRI). This achievement is possible by means of mathematics through spectral analysis of experimentally measured (encoded) time signals from patients as the response to external perturbations by various combinations of magnetic fields. In these, and in many other applications of NMR spectroscopy across interdisciplinary research, as well as in the related technologies, the possibility of reaching deeper conclusions is often severely hampered by the difficulties of performing reliable quantifications and interpretations of the encoded time signals and their computed frequency spectra. Thus e.g. in medical diagnostics, clinicians usually rely upon quantification of a few retrieved metabolite concentrations for the disease assignments [7]. This narrow window, and similar limitations of structural studies in other fields, need to be considerably widened. However, the presence of noise and the underlying reconstruction ambiguities are among the main obstacles to achieve this goal. Such drawbacks can cause an unacceptable omission of one or more physical (genuine) and/or detection of some unphysical (spurious) resonances in spectra in lieu of the sought true constituents of the examined matter.

All the parametric estimators invariably produce extraneous or spurious spectral structures that must confidently be identified to separate the false from the true content of the examined matter [8]–[16]. The entire physical information about different states of a given system is contained in the complete set of genuine poles and zeros of the underlying nodal or fundamental oscillation patterns. Stable physical systems are rooted in these genuine poles and zeros that remain robust against external perturbations. If the fundamental oscillations of a system are going to have a noticeable influence on the performance and/or behavior of this system, their oscillation amplitudes should be different from zero. Spectral peak amplitudes are the Cauchy residues of the system response function, which is driven exclusively by the system poles and zeros. A residue represents a metric defined by the difference/separation between a spectral pole and zero. For generic time signals, the borderline of the unit circle is the natural limit for location of noise in the complex frequency plane. This is a necessary, but not a sufficient condition for signal-noise separation. The reason for this is in a confounding factor: genuine and spurious resonances can be mixed together in the same region.

We presently use the fast Padé transform (FPT) [14]–[16] to tackle the stated obstacles and reconstruction ambiguities. This method unifies the usual Padé approximant (PA) and the Padé $z-$transform (PzT). In signal processing, we are given a set of time signal points $\{c_n\}$, as the expansion coefficients of the input Maclaurin series (Green's or a response function) in powers of the frequency-dependent harmonic variable z^{-1} (Euler's complex exponential). The standard PA to this series is the polynomial quotient in terms of the same variable z^{-1} with the convergence region outside the unit circle ($|z| > 1$). The PzT is an alternative representation of the same Maclaurin series can be given by a different ratio of two other polynomials with the independent variable z and the convergence region inside the unit circle ($|z| < 1$). Upon convergence, the two polynomial quotients from the PA and PzT give the same numerical values. The PzT and PA branches of the FPT are denoted by $\mathrm{FPT}^{(+)}$ and $\mathrm{FPT}^{(-)}$ to make a transparent link to the direct and inverse expansion variables $z^{\pm 1}$, respectively. For a given time signal, the mentioned two polynomial quotients from the FPT give two spectra that coincide with each other when convergence has been reached. These rational polynomials as non-linear response functions are capable of yielding the exact signal-noise separation (SNS). This is due to an unequivocal identification of extraneous resonances through their pole-zero coincidences, and to the corresponding zero amplitudes. Stemming from noise or noise-related information in the input time signal, any ensuing spurious pole in the frequency domain is uniquely detected by Q_K, as being precisely confluent with the associated spurious zero, which is recovered by P_K. Subsequent automatic elimination of this false information from the output data is secured by the very form of the spectrum in the FPT via pole-zero cancellations in P_K/Q_K. Simultaneously, these coincident poles and zeros yield the zero-valued amplitudes, as per the said definition of residues. Such degenerate spectral structures appear as pairs called Froissart doublets [17, 18]. They are spurious because of their demonstrable marked instability against even the weakest external perturbations. Genuine poles and zeros are also detected by Q_K and P_K, respectively, in the FPT through their proven stability and the absence of pole-zero confluences that, in turn, give non-zero amplitudes. Computational illustrations are presently reported confirming the reliability of the FPT in numerically exact reconstructions of spectral parameters for a sufficiently large number of genuine resonances and exact signal-noise separation. It is hoped that these features of the FPT will significantly aid NMR and MRS to reduce the stated limitations and, thus, achieve their full potential. This novel strategy in analysis of spectra by means of the fast Padé transform is by no means limited exclusively to NMR or MRS data. Quite the contrary, the FPT can be used for the most accurate analyses of general spectra that are either experimentally measured or theoretically generated. For example, in the field of atomic, molecular and optical physics, there are many experimental data of various types of Auger and other spectra [19]–[21] that lack reliable quantifications going beyond ambiguous fittings by ad-

justable parameters. Here the fast Padé transform can also be advantageously applied to quantify all physical peaks and/or resonances that could be isolated, overlapping and nearly or completely degenerate. This can be accomplished in the same or a similar way as in our previous studies in medical physics [14]–[16]. Insurmountable difficulties are usually encountered with any estimator based upon fitting the given spectrum because of non-uniqueness of the least-square adjustment to the observed spectral envelope. This is due to the ubiquitous occurrence that any subjectively preassigned number and specific forms of the components of the observed spectral line-shapes can yield practically the same prescribed error. In sharp contrast, the fast Padé transform unequivocally determines the number of the components and the spectral parameters of every physical peak or resonance, as it is illustrated in the present work.

2 Time signals and the physical significance of spectral parameters

Time signals, or equivalently, free induction decay (FID) curves with their fundamental harmonics are spectrally analyzed while solving the quantification problem. The solution of this harmonic inversion problem permits reconstruction of all the physical complex frequencies $\{\omega_k\}$ and the associated complex amplitudes $\{d_k\}$. These spectral parameters are the sole constituents of the fundamental harmonics of the investigated FIDs. Every harmonic represents a transient which possesses its resonant frequency $\mathrm{Re}(\omega_k)$, relaxation time $T_{2k} = \pi^{-1}\mathrm{Im}(\omega_k)$, intensity $|d_k|$ and phase $\phi_k = Arg(d_k)$. Such elements completely determine the underlying normal-mode damped oscillations in the generic signal. These latter four real-valued parameters can be directly deduced from the retrieved complex frequencies and amplitudes to give the peak areas of the associated resonance profiles in the corresponding spectrum.

The physical mechanisms underlying e.g. ICR-MS, NMR, MRS and other fields dictate that the great majority of time signals encountered in vast practice are given by a geometric progression via a sum of powers of K damped complex exponentials $\exp(i\omega_k\tau)$ with fundamental frequencies ω_k and stationary amplitudes d_k according to:

$$c_n = \sum_{k=1}^{K} d_k \, \mathrm{e}^{in\omega_k\tau} \qquad , \qquad \mathrm{Im}(\omega_k) > 0 \qquad (0 \le n \le N-1). \tag{2.1}$$

Given this time signal, the main task of parametric signal processing is to solve the quantification problem by reconstructing the K unknown frequencies and amplitudes $\{\omega_k, d_k\}$, as well as the true number K of genuine resonances.

Recovered fundamental frequencies and amplitudes are used to deduce some other important biophysical and chemical quantities. For example, in clinical diagnostics by means of MRS, the most relevant quantities are metabolite abundance or concentrations that are proportional to the reconstructed peak areas. Metabolite concentrations of the examined tissue can be extracted from spectrally analyzed FIDs. Hence the clinical importance of the quantification problem in MRS. One of the most important aspects of the quantification problem in NMR/MRS is the unequivocal separation of genuine from spurious information. To investigate this problem, we shall presently use the FPT [14]–[16]. Our conclusion about the demonstrated performance of the FPT in MRS are also valid in e.g. analytical chemistry when using ion cyclotron resonance mass spectroscopy (ICRMS) or NMR spectroscopy of various substances or specimens, including large bio-molecules (proteins, peptides, etc), as well as in other applied sciences and technologies with signal processing for data analysis [2].

3 Two variants of the fast Padé transform converging inside and outside the unit circle

For a given time signal $\{c_n\}$ of infinite length $N=\infty$, one defines the exact ideal spectrum via the Green function $G_\infty(z^{-1})$ by the following Maclaurin series in powers of variable z^{-1} :

$$G_\infty(z^{-1})=\lim_{N\to\infty}G_N(z^{-1}) \quad , \quad G_N(z^{-1})=\sum_{n=0}^{N-1}c_n z^{-n}, \tag{3.1}$$

where $z\neq 0$ and $z\neq 1$. The expansion coefficients $\{c_n\}$ are the time signal points, and z is a complex harmonic variable $z=\exp(i\omega\tau)$, where ω is the complex angular frequency with $\mathrm{Im}(\omega)>0$ and τ is the sampling or dwell time. It should be noted that, in practice, N is a finite length for any realistic FID. Thus, the duration of the signal is limited by the total acquisition time T, which is given by $T=N\tau$.

The goal is to find the appropriate method for estimating the infinite sum $G_\infty(z^{-1})$ by using only its finite number of N terms ($N<\infty$) via $G_N(z^{-1})$, which employs the available finite set $\{c_n\}_{n=0}^{N-1}$. This can be achieved by the diagonal FPT in the form of polynomial quotients P_K/Q_K [14]–[16]. In this quotient, the numerator and denominator polynomials can be extracted either analytically or numerically from the available N data points $\{c_n\}$ [2]. The fast Padé transform is applied using the $\mathrm{FPT}^{(+)}$ and $\mathrm{FPT}^{(-)}$, as the two conceptually different and complementary variants, that are introduced by:

$$G_\infty(z) \approx G_K^{\mathrm{FPT}^{(+)}}(z)=\frac{P_K^+(z)}{Q_K^+(z)}=\frac{\sum_{r=1}^{K}p_r^+ z^r}{\sum_{s=0}^{K}q_s^+ z^s}\,, \tag{3.2}$$

$$\approx G_K^{\mathrm{FPT}^{(-)}}(z^{-1})=\frac{P_K^-(z^{-1})}{Q_K^-(z^{-1})}=\frac{\sum_{r=1}^{K}p_r^- z^{-r}}{\sum_{s=0}^{K}q_s^- z^{-s}}\,. \tag{3.3}$$

Note that the numerator polynomial $P_K^+(z)$ in the $\mathrm{FPT}^{(+)}$ from (3.2) and (3.3) does not have its free, constant term i.e. $p_0^+=0$. The plus and minus superscripts in (3.2) and (3.3) denote that the independent variables are $z^{+1}=z$ and z^{-1} are used, respectively. This should be compared to the variable z^{-1} in the input Maclaurin series (3.1).

The polynomial expansion coefficients $\{p_r^\pm, q_s^\pm\}$ are obtained by equating both $G_K^{\mathrm{FPT}^{(+)}}(z)$ as well as $G_K^{\mathrm{FPT}^{(-)}}(z^{-1})$ to the same input series $G_\infty(z^{-1})$ truncated at $n=N-1$. From such approximations, $\sum_{n=0}^{N-1}c_n z^{-n}\approx G_K^{\mathrm{FPT}^{(+)}}(z)$ and $\sum_{n=0}^{N-1}c_n z^{-n}\approx G_K^{\mathrm{FPT}^{(-)}}(z)$, the following two systems of linear equations are to be solved in the $\mathrm{FPT}^{(+)}$ and $\mathrm{FPT}^{(-)}$:

$$\sum_{s=1}^{K}q_s^+ c_{m+s}=-c_m \quad , \quad p_k^+=\sum_{r=0}^{K-k}c_r q_{r+k}^+ \qquad (0\le m\le L, 1\le k\le K)\,, \tag{3.4}$$

$$\sum_{s=1}^{K}q_s^- c_{K+m-s}=-c_{K+m} \quad , \quad p_k^-=\sum_{r=0}^{k}c_r q_{k-r}^- \qquad (1\le m\le L, 0\le k\le K)\,, \tag{3.5}$$

where $q_0^\pm=1$ and $L=N-K-1$. In (3.4) for the $\mathrm{FPT}^{(+)}$, albeit coupled, the two systems for $\{q_r^+\}$ and $\{p_k^+\}$ need not be solved at the same time. Since the coupling is sequential, the system for the unknowns $\{q_s^+\}$ can be solved first without referring to the other unknowns $\{p_k^+\}$. Furthermore, once the set $\{q_s^+\}$ becomes available, the remaining system need not be solved at all, because the expression $p_k^+=\sum_{r=0}^{K-k}c_r q_{r+k}^+$ is itself the solution for $\{p_k^+\}$. An entirely similar situation is encountered in the $\mathrm{FPT}^{(-)}$ when dealing with the two systems of linear equations for

$\{q_s^-\}$ and $\{p_r^-\}$ from (3.5), The system of equations for $\{q_r^+\}$, as well as $\{q_r^-\}$ can be solved in a highly accurate manner via various powerful algorithms of linear algebra optimized by e.g. the singular value decomposition (SVD) to refine the solutions for these expansion coefficients of the Padé polynomials $P_K^\pm$ and $Q_K^\pm$ [2]. The veracity of the ensuing results can be checked against the values obtained from the analytical formulae for the general coefficients $\{p_r^\pm, q_s^\pm\}$ [2].

By definition, the FPT$^{(+)}$ and FPT$^{(-)}$ have their convergence regions inside ($|z| < 1$) and outside ($|z| > 1$) the unit circle, respectively. The convergence range of the input series $G_\infty(z^{-1})$ from (3.1) is outside the unit circle $|z| > 1$. Thus, he same series $G_\infty(z^{-1})$ diverges inside the unit circle $|z| < 1$. As such, the FPT$^{(-)}$ accelerates the already convergent series $G_\infty(z^{-1})$ for $|z| > 1$. On the other hand, the FPT$^{(+)}$ induces convergence into the divergent series $G_\infty(z^{-1})$ for $|z| < 1$. By reference the Cauchy analytical continuation, both FPT$^{(+)}$ and FPT$^{(-)}$ are valid throughout the complex plane with the exception of poles $z^{\pm 1} = z_k^{\pm 1}$. However, in practice, one computes spectra at real frequencies ω so that we always have $z^{\pm 1} \neq z_k^{\pm 1}$ for complex-valued $\{\omega_k^\pm\}$. As such the Padé spectra $P_K^\pm(z^{\pm 1})Q_K^\pm(z^{\pm 1})$ are well defined even at all their poles $\{\omega_k^\pm\}$.

The task of the FPT$^{(+)}$ is more demanding than that of the FPT$^{(-)}$ due to conversion of divergence into convergence through analytical continuation by way of numerical computations. However, the results from the FPT$^{(+)}$ do coincide with those from the FPT$^{(-)}$ at full convergence of both variants. This is related to the fact which is well-known from the foundation of the Padé approximant, namely, that for a given series, such as the Maclaurin expansion from (3.1), there is only one polynomial quotient. Thus, due to this uniqueness of the FPT, all the results from the FPT$^{(+)}$ and FPT$^{(-)}$ must coincide after convergence has occurred. The FPT$^{(+)}$ and FPT$^{(-)}$ converge to their respective limiting values from two diametrically opposite directions with respect to the circumference of the unit circle $|z| = 1$. Therefore, the uniqueness of the FPT guarantees that the findings from the FPT$^{(+)}$ and FPT$^{(-)}$ must be in full agreement up to the difference of the order of the background noise. This is confirmed by our computations.

4 Reconstruction of complex frequencies and amplitudes by FPT

It can be seen from (3.3) and (3.4) that the complex-valued spectra in the FPT$^{(\pm)}$ are defined by rational polynomials $P_K^\pm(z^{\pm 1})/Q_K^\pm(z^{\pm 1})$ in the FPT$^{(\pm)}$ that lead to the peaks at the zeros. The numerator $P_K^\pm(z^{\pm 1})$ and denominator $Q_K^\pm(z^{\pm 1})$ polynomials enable the FPT to provide the exact separation of genuine (physical) from spurious (unphysical, noise and/or noise-like) information encountered either in theory or measurements involving time signals. This is accomplished by means of Froissart doublets [17] that are coincident pairs of poles $z_k^{\pm 1} \equiv z_{k,Q}^\pm$ and zeros $z_{k,P}^\pm$ in the response functions $P_K^\pm(z^{\pm 1})/Q_K^\pm(z^{\pm 1})$ from the FPT$^{(\pm)}$. Here, $z_{k,P}^\pm$ and $z_{k,Q}^\pm$ are the solutions of the numerator and denominator characteristic or secular equations:

$$P_K^\pm(z_{k,P}^\pm) = 0 \quad , \quad z_{k,P}^\pm = \mathrm{e}^{\pm i\omega_{k,P}^\pm \tau}, \tag{4.1}$$

$$Q_K^\pm(z_{k,Q}^\pm) = 0 \quad , \quad z_{k,Q}^\pm = \mathrm{e}^{\pm i\omega_{k,Q}^\pm \tau}. \tag{4.2}$$

The subscripts P and Q in the spectral zeros $z_{k,P}^\pm$ and poles $z_{k,Q}^\pm$ are introduced to remind us that they are the roots of the characteristic equations (4.1) and (4.2) for the numerator $P_K^\pm(z_k^\pm)$ and denominator $Q_K^\pm(z_k^\pm)$ polynomials, respectively. Froissart pole-zero confluences are synchronized with the corresponding zero values obtained for Froissart amplitudes:

$$\text{Spurious}: \quad z_{k,Q}^\pm = z_{k,P}^\pm \quad \therefore \quad \{d_k^\pm\}_{z_{k,Q}^\pm = z_{k,P}^\pm} = 0. \tag{4.3}$$

By changing the degree K of the polynomials in the diagonal FPT$^{(\pm)}$ from $P_K^\pm(z^{\pm 1})/Q_K^\pm(z^{\pm 1})$, Froissart doublets unpredictably and uncontrollably alter their positions in the complex $z^{\pm 1}-$planes.

They never converge (stabilize) even when the whole signal length is exhausted. Therefore, these latter resonances that roam around in the complex planes are considered as spurious or unphysical. As such, unstable resonances are identified by their twofold signature: pole-zero coincidences and zero amplitudes for noise-free time signals. The same type of signature also applies to noise-corrupted time signals (theoretically generated or experimentally measured). The only difference is that, in this case, instead of numerically exact equalities from (4.3), we shall have the approximations $z^{\pm}_{k,Q} \approx z^{\pm}_{k,P}$ and $d^{\pm}_{k} \approx 0$. Crucially, however, although Froissart doublets are unstable against even the smallest external perturbation (e.g., altering the degree of the Padé polynomial, adding noise, etc), they nevertheless consistently preserve the relationships in (4.3) or $z^{\pm}_{k,Q} \approx z^{\pm}_{k,P}$ and $d^{\pm}_{k} \approx 0$.

By contrast, there are retrieved resonances with spectral parameters that converge. These are viewed as stable, genuine or physical resonances. The signatures of all such genuine resonances are:

$$\text{Genuine}: \quad z^{\pm}_{k,Q} \neq z^{\pm}_{k,P} \quad \therefore \quad \{d^{\pm}_{k}\}_{z^{\pm}_{k,Q} \neq z^{\pm}_{k,P}} \neq 0. \tag{4.4}$$

Amplitudes $d^{\pm}_{k}$ are the Cauchy residues of quotients $P^{\pm}_{K}(z^{\pm 1})/Q^{\pm}_{K}(z^{\pm 1})$ taken at the poles $z^{\pm}_{k,Q}$. Here, the word residues has the transparent meaning of the residual differences which remain after the values of the poles are subtracted from the zeros, implying that $d^{\pm}_{k}$ are proportional to $z^{\pm}_{k,Q} - z^{\pm}_{k,P}$ in the sense of a metric via $d^{\pm}_{k} \propto (z^{\pm}_{k,Q} - z^{\pm}_{k,P})$. Thus, the distances between poles $z^{\pm}_{k,Q}$ and zeros $z^{\pm}_{k,P}$ are proportional to the amplitudes $d^{\pm}_{k}$. Hence $d^{\pm}_{k} \equiv 0$ for the exact pole-zero coincidences in the Froissart doublets (4.3).

It is vital to have full control over the locations of all the zeros of $Q^{\pm}_{K}(z^{\pm 1})$ in the Padé quotients $P^{\pm}_{K}(z^{\pm 1})/Q^{\pm}_{K}(z^{\pm 1})$ from the FPT$^{(\pm)}$. Such control is possible in the FPT$^{(+)}$ and FPT$^{(-)}$ because all the genuine zeros of $Q^{+}_{K}(z)$ and $Q^{-}_{K}(z^{-1})$ are inside and outside the unit circle, respectively. However, despite our prior knowledge about such precise locations before reconstructing these zeros, as soon as the systematically increased degree K of $Q^{\pm}_{K}(z^{\pm 1})$ surpasses the unknown true order $K_{\rm G}$, spurious roots $\{z^{\pm}_{k,Q}\}$ of the characteristic equations $Q^{\pm}_{K}(z^{\pm 1}) = 0$ would inevitably appear. For the same reason, spurious zeros $\{z^{\pm}_{k,P}\}$ will also emerge from the accompanying secular equations of the numerator polynomials $P^{\pm}_{K}(z^{\pm 1}) = 0$. This is where the Froissart concept comes into play to take advantage of the spuriousness in the set $\{z^{\pm}_{k,Q}\}$. Namely, the two types of spuriousness from the two sources $Q^{\pm}_{K}(z^{\pm 1}) = 0$ and $P^{\pm}_{K}(z^{\pm 1}) = 0$ are strongly coupled together. As a result, spurious Froissart poles $\{z^{\pm}_{k,Q}\}$ and zeros $\{z^{\pm}_{k,P}\}$ are always born out as pairs. It is in this way that Froissart doublets manifest themselves through pole-zero coincidences, $\{z^{\pm}_{k,Q}\} = \{z^{\pm}_{k,P}\}$, as in (4.3). Such an occurrence cancels the entire spuriousness from the polynomial quotients $P^{\pm}_{K}(z^{\pm 1})/Q^{\pm}_{K}(z^{\pm 1})$. This becomes particularly apparent when these ratios are written in their canonical forms:

$$\frac{P^{\pm}_{K}(z^{\pm 1})}{Q^{\pm}_{K}(z^{\pm 1})} = \frac{p^{\pm}_{K}}{q^{\pm}_{K}} \prod_{k=1}^{K} \frac{(z^{\pm 1} - z^{\pm}_{k,P})}{(z^{\pm 1} - z^{\pm}_{k,Q})}. \tag{4.5}$$

If the running degree K is larger than the number of genuine resonances $K_{\rm G}$, then all the terms $(z^{\pm 1} - z^{\pm}_{k,P})/(z^{\pm 1} - z^{\pm}_{k,Q})$ from (4.5) for $K - K_{\rm G} > 0$ would contain spurious Froissart poles $z^{\pm}_{k,Q}$ and zeros $z^{\pm}_{k,P}$. Hence pole-zero cancellations leading to $(z^{\pm 1} - z^{\pm}_{k,P})/(z^{\pm 1} - z^{\pm}_{k,Q}) = 1$ for Froissart doublets $z^{\pm}_{k,Q} = z^{\pm}_{k,P}$, as per (4.3).

The ensuing consequence of these pole-zero cancellations onto the corresponding amplitudes of Froissart resonances can be seen at once from the explicit formulae for $d^{\pm}_{k}$ in terms of all the recovered poles and zeros:

$$d^{\pm}_{k} = \frac{p^{\pm}_{K}}{q^{\pm}_{K}} \prod_{k'=1}^{K} \frac{(z^{\pm}_{k,Q} - z^{\pm}_{k',P})}{(z^{\pm}_{k,Q} - z^{\pm}_{k',Q})}_{k' \neq k}. \tag{4.6}$$

Here, in the numerator, it is permitted to have $k' = k$, in which case every Froissart doublet from (4.3) would produce zero-valued terms $(z^{\pm}_{k,Q} - z^{\pm}_{k,P})$ and, thus, the whole product in (4.6) will become zero. As mentioned, this yields $d^{\pm}_k = 0$ for $z^{\pm}_{k,Q} = z^{\pm}_{k,P}$, according to (4.3). In computations, expression (4.6) should not be used to obtain the amplitudes $d^{\pm}_k$ in the FPT$^{(\pm)}$. This is because formula (4.6) employs the whole set of the reconstructed amplitudes to compute $d^{\pm}_k$ for the k th resonance. Therefore, even the slightest inaccuracy, such as near cancellations of poles and zeros, rather than the theoretically exact cancellations, could spoil the precision of the sought $d^{\pm}_k$ for the given k. Instead, we use the alternative and equivalent expressions:

$$d^{\pm}_k = \lim_{z^{\pm 1} \to z^{\pm}_{k,Q}} \left\{ (z^{\pm 1} - z^{\pm 1}_k) \frac{P^{\pm}_K(z^{\pm 1})}{Q^{\pm}_K(z^{\pm 1})} \right\} = \frac{P^{\pm}_K(z^{\pm}_{k,Q})}{Q^{\pm}_K{}'(z^{\pm}_{k,Q})} \qquad ; \qquad Q^{\pm}_K{}'(z^{\pm}_{k,Q}) \neq 0, \tag{4.7}$$

where $Q^{\pm}_K{}'(z^{\pm 1}) = (\mathrm{d}/\mathrm{d}z^{\pm 1}) Q^{\pm}_K(z^{\pm 1})$. Here, each k th amplitude on the lhs depends only on one, i.e., the k th value of the rhs of Eq.(4.6) and, hence, no other resonance can deteriorate the accuracy of the retrieved $d^{\pm}_k$.

In summary, the FPT$^{(\pm)}$can carry out the exact numerical reconstruction of all the spectral fundamental frequencies $\{\omega^{\pm}_k\}$ and amplitudes $\{d^{\pm}_k\}$, with minimal computational effort. We only need to solve one system of linear equations for the expansion coefficients of the denominator polynomial which is afterwards rooted. Rooting as the only non-linear operation can be avoided altogether by resorting to a linear algorithm which solves the equivalent eigenvalue problem with the corresponding sparse Hessenberg matrix [22]. Due to their variational nature, the FPT$^{(+)}$ and FPT$^{(-)}$ yield the upper and the lower bounds $\{\omega^{+}_k, d^{+}_k\}$ and $\{\omega^{-}_k, d^{-}_k\}$ of the exact spectral parameters $\{\omega_k, d_k\}$. The absorption spectra in the FPT$^{(\pm)}$ are defined by the real parts of the corresponding complex spectra $\mathrm{Re}(G^{\mathrm{FPT}^{(\pm)}}_K(z^{\pm 1}))$. The envelope spectra can be computed in the FPT without any spectral parameters. This is accomplished using only the polynomial quotients in (3.3) and (3.4). For quantification by the FPT, computations of the frequencies and amplitudes $\{\omega^{\pm}_k, d^{\pm}_k\}$ are carried out by the explained procedure of spectral analysis.

Overall, it is clear from these remarks that the FPT$^{(\pm)}$ possess a very elegant, simple and powerful solution for the exact identification of all spurious Froissart resonances [4]. When these are discarded, only genuine resonances are left in the output line-list of the reconstructed spectral parameters. This yields the exact solution of the quantification problem. In the next section, we shall illustrate the performance of the FPT on the theoretical and experimental for time signals from MRS. Similar applications can be done using many other time signals and spectra encountered across interdisciplinary research, including atomic and molecular spectroscopy [19]–[21].

A time signal described by a linear combination of K complex damped exponentials (2.1) gives a spectrum as a sum of K complex Lorentzians. The real part of each Lorentzian has dispersion-type Breit-Wigner form which is known from theory of resonant scattering. In practice, various imperfections in experimental encoding time signals (static magnetic field inhomogeneity, shimming, etc) [23] may lead to certain departures from Eq. (2.1). In the MRS literature, such deviations are often modeled through multiplication of all exponentials in Eq. (2.1) by the associated time dependent Gaussians. In the frequency domain, this yields a convolution of Lorentzians by Gaussians, and such a function is known as the frequency Voigt profile. Its inverse Fourier integral gives the time Voigt profile which has the form $\exp(-\alpha t - \beta t^2)$ where α and β are real positive constants [2]. The FPT can be extended to treat any lineshape, including the Voigt profile. This can be done whenever the given profile possess a power series expansion, which can be readily combined with the Maclaurin series (3.1) to generate the Padé numerator and denominator polynomials by means of either Rutishauser's quotient-difference or Gordon's product-difference algorithms [2]. The present computations within spectral analysis for the brain MRS will employ Lorentzians in order to have a clear illustrations of pole-zero coincidences with precisely delineated Froissart doublets for exact

Table 1. Numerical values for all the input spectral parameters: the real $\mathrm{Re}(\nu_k)$ and imaginary $\mathrm{Im}(\nu_k)$ parts of the complex frequencies ν_k, and the absolute values $|d_k|$ of the complex amplitudes d_k of 25 damped complex exponentials from the synthesized time signal (2.1) similar to those encoded clinically by MRS at the magnetic field strength $B_0 = 1.5$T from a healthy human brain [24]. Every phase $\{\phi_k\}$ of the amplitudes is set to zero, i.e., each d_k is chosen as purely real, $d_k = |d_k| \exp(i\phi_k) = |d_k|$. The letter M_k denotes the kth metabolite.

INPUT DATA : ALL SPECTRAL PARAMETERS of the TIME SIGNAL or FID

n_k°	$\mathrm{Re}(\nu_k)$ (ppm)	$\mathrm{Im}(\nu_k)$ (ppm)	$\lvert d_k \rvert$ (au)	M_k
1	0.985	0.180	0.122	Lip
2	1.112	0.257	0.161	Lip
3	1.548	0.172	0.135	Lip
4	1.689	0.118	0.034	Lip
5	1.959	0.062	0.056	Gaba
6	2.065	0.031	0.171	NAA
7	2.145	0.050	0.116	NAAG
8	2.261	0.062	0.092	Gaba
9	2.411	0.062	0.085	Glu
10	2.519	0.036	0.037	Gln
11	2.675	0.033	0.008	Asp
12	2.676	0.062	0.063	NAA
13	2.855	0.016	0.005	Asp
14	3.009	0.064	0.065	Cr
15	3.067	0.036	0.101	PCr
16	3.239	0.050	0.096	Cho
17	3.301	0.064	0.065	PCho
18	3.481	0.031	0.011	Tau
19	3.584	0.028	0.036	m−Ins
20	3.694	0.036	0.041	Glu
21	3.803	0.024	0.031	Gln
22	3.944	0.042	0.068	Cr
23	3.965	0.062	0.013	PCr
24	4.271	0.055	0.016	PCho
25	4.680	0.108	0.057	Water

signal-noise separation exhibited in the Padé polynomial quotients (3.4) and (3.5). The use of Voigtians will be illustrated in a general context of state survival probabilities for systems exposed to external fields with an important application to radiobiology [3, 4].

5 Results

Table 1 gives the input data for the quantification problem to be solved in the present work. These data are the complex fundamental frequencies and the corresponding amplitudes from a synthesized noise-free time signal (2.1), whose associated spectrum is comprised of a total of 25 resonances, some of which are individual although tightly packed peaks, while others are closely-overlapped or nearly degenerate. The numerical values of the spectral parameters were chosen to correspond to the typical frequencies and amplitudes found in proton MR time signals encoded *in vivo* from a healthy human brain at 1.5T [24]. The columns in Table 1 of the input fundamental harmonics are headed by labels n_k°, $\mathrm{Re}(\nu_k)$ (ppm), $\mathrm{Im}(\nu_k)$ (ppm), $|d_k|$ (au) and M_k that represent the running number, real and imaginary frequencies (both in parts per million, ppm), absolute values of amplitudes (in arbitrary units, au) and the metabolite assignments, respectively. Of particular note are the crossings of the 2nd column with the 11th and 12th rows where the two chemical shifts $\mathrm{Re}(\nu_{11})$ and $\mathrm{Re}(\nu_{12})$ have a small splitting, $\mathrm{Re}(\nu_{12}) - \mathrm{Re}(\nu_{11}) = 0.001$ ppm.

The specifics of the present model for noise run as follows. We add random numbers $\{r_n\}$ to the mentioned noiseless time signal $\{c_n\}$ to generate the noisy input data $\{c_n + r_n\}\,(0 \le n \le N-1)$. More precisely, this additive noise r_n is a set $\{r_n\}\,(0 \le n \le N-1)$ of N random Gauss-distributed zero mean numbers (orthogonal in the real and imaginary parts) with the standard deviation $\sigma = \lambda \times \mathrm{RMS}$. Here, λ is the selected noise level and the acronym RMS stands for root-mean-square (or equivalently, the quadratic mean) of the noiseless time signal. For the given noiseless set $\{|c_n|\}$ generated with the spectral parameters from Table 1, RMS is defined by the arithmetic mean (average) value $\mathrm{RMS} = (\sum_{n=0}^{N} |c_n|^2/N)^{1/2}$. According to this noise model, adding $\lambda\,\%$ noise $\{r_n\}$ to noiseless data $\{c_n\}$ of $\mathrm{RMS}_{\mathrm{noise-free}}$ would produce noisy data $\{c_n + r_n\}$ whose $\mathrm{RMS}_{\mathrm{noise-corrupted}}$ is $\lambda\,\%$ of $\mathrm{RMS}_{\mathrm{noise-free}}$, so that $\mathrm{RMS}_{\mathrm{noise-corrupted}} = \lambda\,\mathrm{RMS}_{\mathrm{noise-free}}$. Here λ is a fixed number expressed in percent. For example, adding 10% noise would yield a new RMS (noisy), which is 10% of the old RMS (noiseless), $\sigma = 0.01\,\mathrm{RMS}_{\mathrm{noise-free}}$. In the present computations, we shall fix the noise level λ to be a constant number equal to 0.00289, so that $\sigma = 0.00289\,\mathrm{RMS}$ where, as stated, $\mathrm{RMS} \equiv \mathrm{RMS}_{\mathrm{noise-free}}$. The value 0.00289 in the standard deviation σ of noise is chosen to approximately match 1.5% of the height of the weakest resonance ($n_k^\circ = 13$) in the spectrum. Such a noise level is sufficient to illustrate the main principles of Froissart doublets. However, the Padé-based processing can successfully handle spectra and images with much higher noise levels in simulated and encoded data as previously been [14]–[16].

Figure 1 illustrates the reason for which mathematical methods are indispensable in MRS and many other fields that rely upon signal processing. The top panel (i) in this figure depicts the time signal from the input data that are reminiscent of those encoded *vivo* by means of MRS from the grey matter of the healthy human brain. The shown free induction decay curve is heavily packed with exponentially decaying oscillations and no other discernable structure appear. Specifically, it is impossible to decipher any physically meaningful information by inspecting any FID directly in the measured time domain. However, from such a time signal one can compute an MR spectrum which exhibits the definite advantage of displaying a relatively small number of distinct characteristics that are amenable to further analyses and interpretations for practical purposes. A typical total shape spectrum of this type is shown in the middle panel (ii) in Fig. 1 in the absorption mode.

This is obtained by a simple and powerful mathematical transformation of the original time signal into its dual or complementary representation in the frequency domain. The advantage of this passage to the frequency representation is manifested in the emergence of a number of clearly discernable features through the appearance of peaks and valleys. Nevertheless, the total shape spectrum is merely an envelope which, at best, could provide only qualitative information about the overall contribution from the sum of all the constituent resonances, but not the individual components themselves that are seen on panel (iii) in Fig. 1, as reconstructed by the $\mathrm{FPT}^{(-)}$. Thus, despite being much more revealing than the time signal, the spectral envelope from panel (ii) is still only qualitative as well as inconclusive and, as such, often of limited practical usefulness. Yet, the FFT, as the most frequently used signal processor in many inter-disciplinary applications, including ICR-MS, NMR and MRS, is restricted to computations of total shape spectra alone.

Overall, the absorption total shape spectra cannot directly provide the information about any feature of resonances, such as the most important abundance/concentrations of the underlying molecules of the examined substance. Indirect information is often surmised from these spectral Fourier-type envelopes by attempting to fit a subjectively preassigned number of resonances hidden beneath each peak structure. The most serious of these drawbacks is non-uniqueness, which stems from the fact that virtually any chosen number of components could equally well produce an acceptable error in the conventional least-square adjustments to the given spectral envelope. Hence, for practical purposes, it would be far more advantageous to have an alternative mathematical transformation, which would use only the original, unedited, raw time signal to first obtain the unique spectral parameters of each peak (position, width, height, phase) and then to generate the

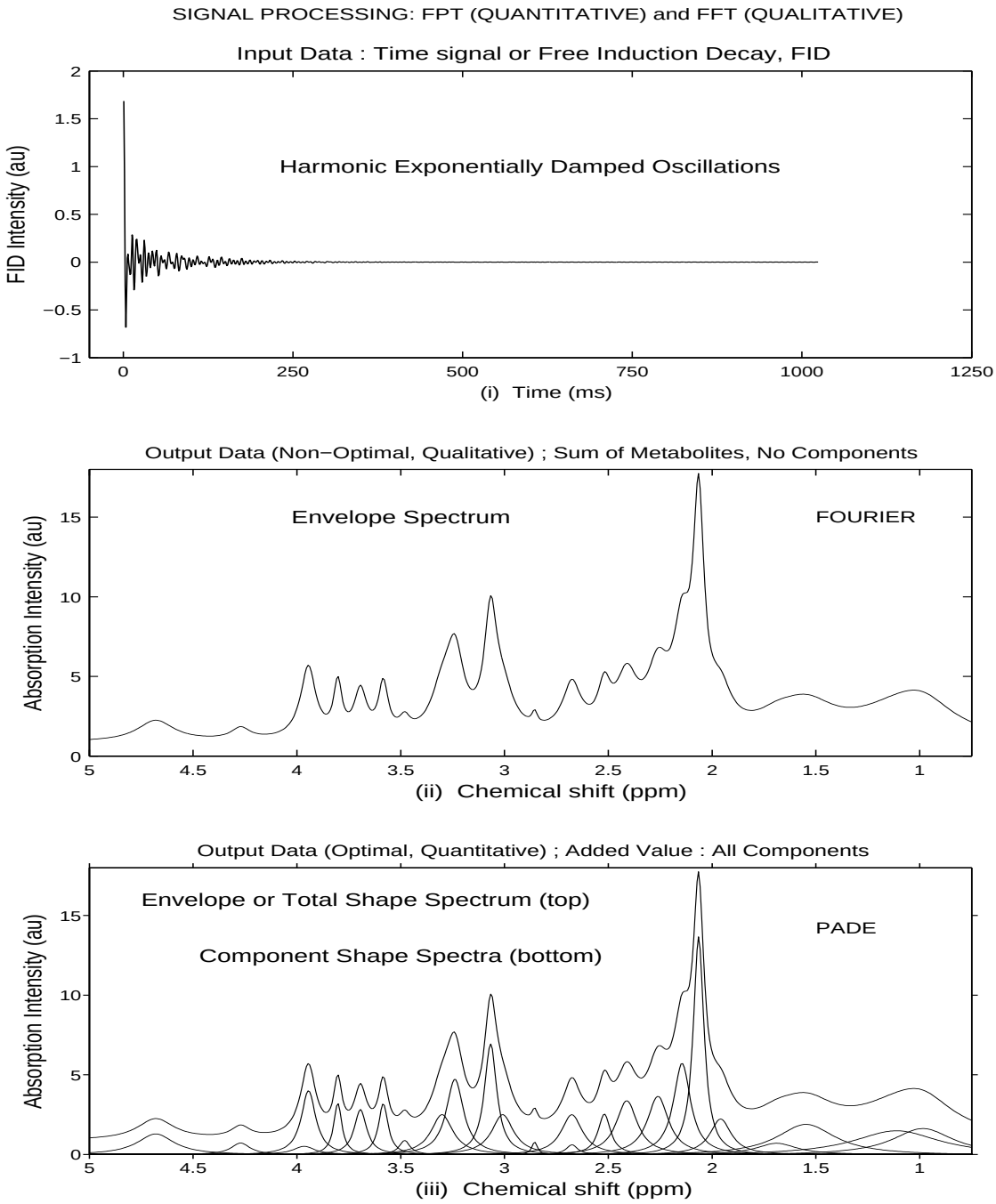

Figure 1: Time and frequency domain data in signal processing in the noiseless case using the fast Fourier transform (FFT) and fast Padé transform (FPT). Top panel (i): the input FID (to avoid clutter, only the real part of the time signal is shown). Middle panel (ii): absorption total shape spectrum (FFT). Bottom panel (iii): absorption component (lower curves; FPT) and total (upper curve; FPT) shape spectra. Panels (ii) and (iii) are generated using both the real and imaginary parts of the FID.

component and total shape spectra in any of the selected modes (absorption, dispersion, magnitude, power). Nevertheless, such spectra with curves, although convenient, are only for visual inspection.

The most important are the numerical values of the recovered spectral parameters and especially molecular concentrations. The reason for this is that, when analyzing experimentally measured FIDs, it is only with these numbers from tables (rather than with envelopes from graphs) that the adequate quantitative assessment could be made as to which molecule do and which do not have their normal concentrations. Here the word "normal" in the case of the scanned human organ by means of MRS relates to a healthy tissue. To achieve this goal, the mentioned advanced mathematical methods must unambiguously separate the physical from non-physical (noise, noise-like) contents in the input time-domain data, to reconstruct exactly the true number of individual resonances and, finally, to deduce the concentrations of every physical molecule. The signal processor capable of fulfilling all these most stringent physical for versatile practical applications, including MRS in medical diagnostics, is the fast Padé transform. The FPT yields the unique component shape spectra as on panel (iii) in Fig. 1. Such component spectra are used to subsequently generate the associated exact envelope. This is opposed to all fitting routines which start from the Fourier envelope spectrum and try to guess the component spectra.

Signal-noise separation by means of Froissart doublets within the $\mathrm{FPT}^{(+)}$ and $\mathrm{FPT}^{(-)}$ is illustrated in Figs. 2 and 3 for the noise-free and noise-corrupted time signals, respectively. All the retrieved genuine resonances as well as Froissart doublets as spurious resonances are detected by the confluence of poles and zeros in the list of the Padé-reconstructed spectral parameters. It is seen on panel (i) in Figs. 2 and 3 that the $\mathrm{FPT}^{(+)}$ disentangles the physical from unphysical resonances by the opposite signs of their imaginary frequencies $\mathrm{Im}(\nu_k^{\pm}) > 0$ and $\mathrm{Im}(\nu_k^{\pm}) < 0$, respectively. In other words, the $\mathrm{FPT}^{(+)}$ provides the exact separation of the genuine from any spurious contents of the investigated noiseless and noisy time signals. On the other hand, in the $\mathrm{FPT}^{(-)}$ depicted on panel (ii) in Figs. 2 and 3, genuine and spurious resonances are mixed together, since they all have the same positive sign of their imaginary frequencies, $\mathrm{Im}(\nu_k^{\pm}) > 0$. Nevertheless, the emergence of Froissart doublets also remains evidently clear in the $\mathrm{FPT}^{(-)}$ via coincidence of poles and zeros, with the ensuing unambiguous identification of spurious resonances. Precisely due to pole-zero coincidences, each Froissart doublet has zero-valued amplitudes, as seen on panel (iii) in Figs. 2 and 3. This result, as another signature of Froissart doublets, represents a further check of consistency and fidelity of separation of genuine from spurious resonances within the concept of SNS.

As seen in Fig. 2, Froissart doublets for the noise-free time signal are all regularly aligned/chained practically throughout the whole Nyquist range. On the other hand, in Fig. 3, Froissart doublets for the noise-corrupted time signal are irregularly distributed in an unpredictable, chaotic, random fashion. A marked instability of Froissart doublets is rooted in their feeble amplitudes. As such, coincident poles and zeros that, as unstable pairs, constitute Froissart doublets possess the amplitudes which are either strictly zero for synthesized FIDs or nearly zero for measured FIDs. Pole-zero confluences and vanishingly small amplitudes jointly represent one of the most prominent signatures of noise and/or noise-like content of FIDs and the corresponding spectra. This is in sharp contrast to the genuine, physical resonances that are stable, since they largely insensitive to various perturbations. As can be observed in Figs. 2 and 3, physical resonances are located in the frequency range [0.984 (Lipids),4.68 (Water)] ppm. Spurious resonances are predominantly outside the latter interval. As such, there is a minimal overlap between the unphysical and physical resonances. It appears as if the physical resonances "repel" the unphysical ones (Froissart) on Figs. 2 and 3. In the $\mathrm{FPT}^{(+)}$, which is initially defined with the convergence inside the unit circle, the genuine and spurious resonances are completely separated from each other, since they have opposite signs of their imaginary frequencies (top panel (i) on Figs. 2 and 3. However, in the $\mathrm{FPT}^{(-)}$, which is initially defined with the convergence outside the unit circle, the genuine and spurious resonances have the same sign of their imaginary frequencies (middle panel (ii) on Figs.

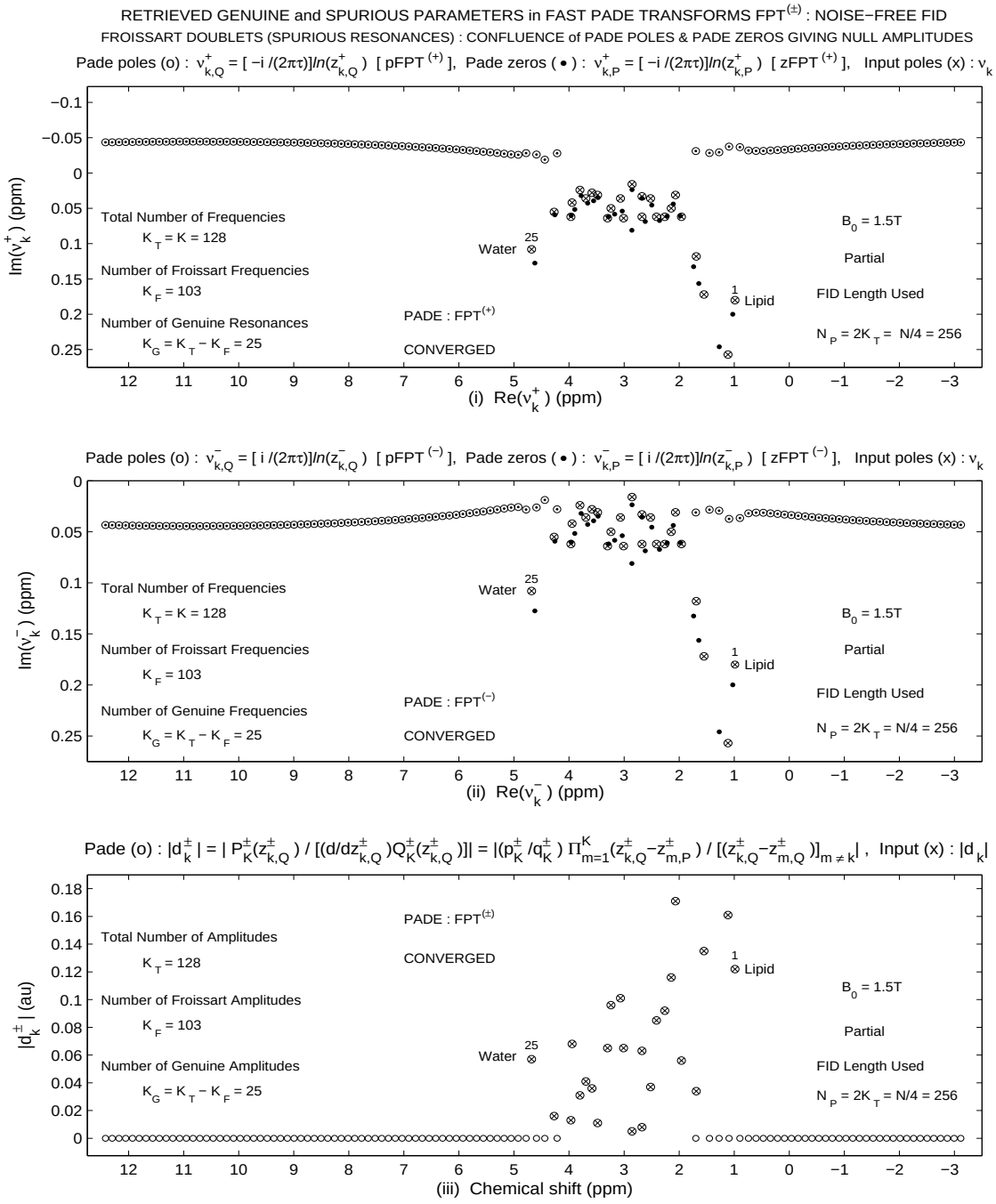

Figure 2: The whole Nyquist frequency interval with the full set of Froissart doublets alongside all the spectral parameters (fundamental frequencies and amplitudes) of genuine resonances retrieved by the FPT$^{(\pm)}$ at a quarter ($N/4 = 256$) of the full length ($N = 1024$) of a noise-free time signal. On panel (i), the FPT$^{(+)}$ achieves a total separation of genuine from spurious resonances that are mixed together in the FPT$^{(-)}$ on panel (ii). Panel (iii) shows genuine and spurious amplitudes in the FPT$^{(\pm)}$. The reconstructed converged amplitudes are identical in the FPT$^{(+)}$ and FPT$^{(-)}$. All the spurious amplitudes are zero-valued.

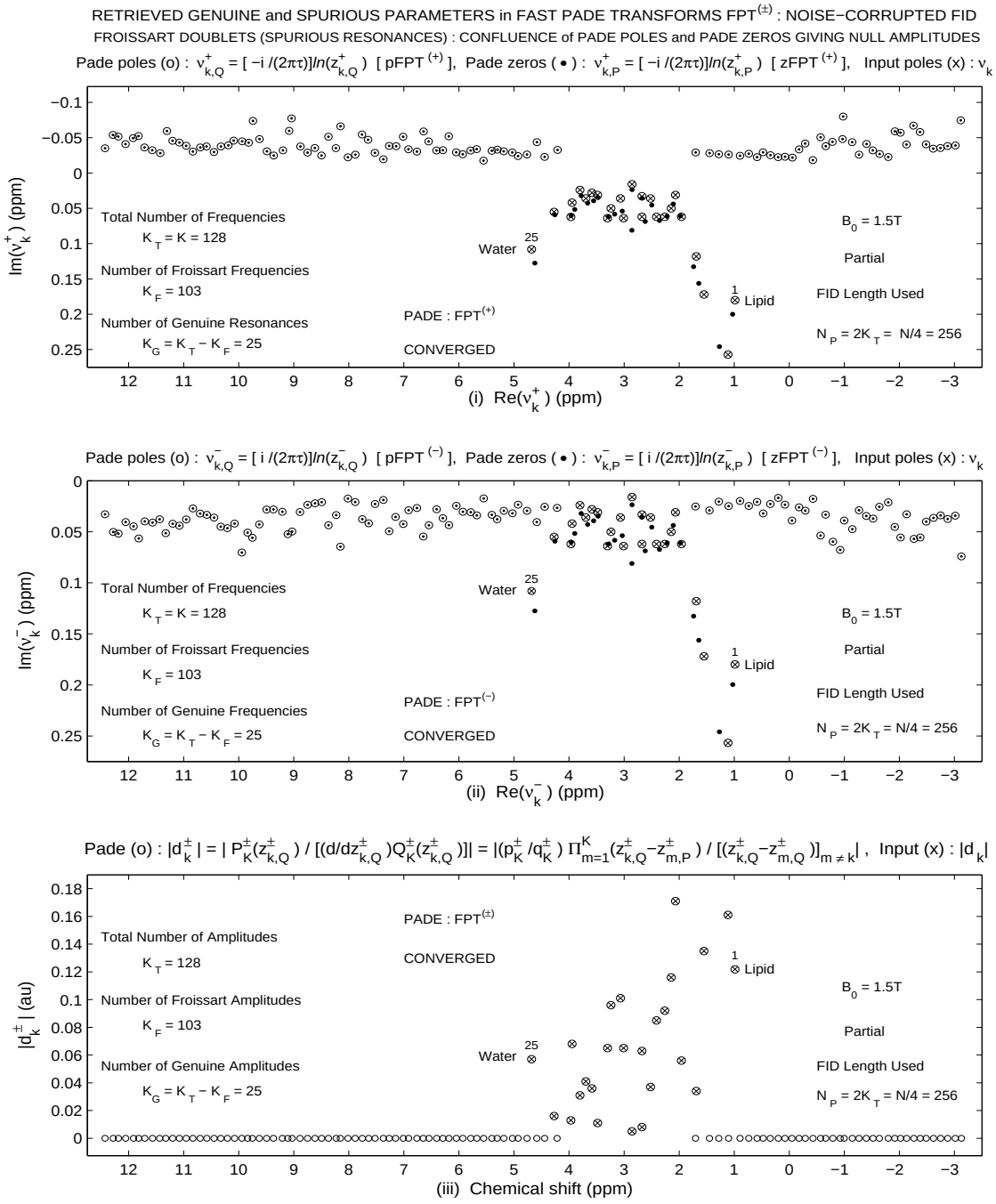

Figure 3: The whole Nyquist frequency interval with the full set of Froissart doublets together with all the spectral parameters (fundamental frequencies and amplitudes) of genuine resonances recovered by the FPT$^{(\pm)}$ at a quarter ($N/4 = 256$) of the full length ($N = 1024$) of a noise-corrupted time signal. On panel (i), the FPT$^{(+)}$ achieves a total separation of genuine from spurious resonances that are mixed together in the FPT$^{(-)}$ on panel (ii). Panel (iii) shows genuine and spurious amplitudes in the FPT$^{(\pm)}$. The reconstructed converged amplitudes are identical in the FPT$^{(+)}$ and FPT$^{(-)}$. All the spurious amplitudes are zero-valued.

2 and 3). Crucially, for both variants, FPT$^{(+)}$ and FPT$^{(-)}$, signal and noise can unambiguously be separated by the confluence of poles and zeros in Froissart doublets as well as by the ensuing zero-valued amplitudes (bottom panel (iii) on Figs. 2 and 3).

Once the Froissart doublets are identified and discarded from the whole set of the results, only the reconstructed parameters of the genuine resonances will remain in the output data. The latter set of Padé-retrieved spectral parameters also contains the exact number K_G of genuine resonances as the difference between the total number K of all the found resonances and the number K_F of Froissart doublets, $K_G = K - K_F$. In Figs. 2 and 3, we used a quarter of the full signal length $N_P = N/4 = 1024/4 = 256$, which corresponds to the Padé polynomial degree $K = 128$ in spectra $P_K^{\pm}/Q_K^{\pm}$. As seen on Figs. 2 and 3, In the whole Nyquist range, as seen on Figs. 2 and 3, the FPT$^{(+)}$ and FPT$^{(-)}$ find 103 Froissart doublets ($K_F = 103$). Therefore, the number K_G of genuine resonances reconstructed by the FPT$^{(+)}$ and FPT$^{(-)}$ is given by $K_G = 128 - 103 = 25$, in exact agreement with the corresponding value of the input data. These illustrations confirm that Froissart doublets simultaneously achieve three important goals: (i) noise reduction, (ii) dimensionality reduction and (iii) stability enhancement. Stability against perturbations of the physical time signal under study is critical to the reliability of spectral analysis. The main contributor to instability of systems is its spurious content. Being inherently unstable and incoherent, spuriousness is unambiguously identified by the twofold signature of Froissart doublets (pole-zero coincidences and zero-valued amplitudes) and, as such, discarded from the output data in the FPT. What is left is genuine information alone which is stable and coherent.

Overall, small amplitudes are the cause for great instability of spurious resonances i.e. Froissart doublets. This is opposed to stability of genuine resonances. Such a diametrically opposite behavior of physical and unphysical resonances greatly facilitates the task of distinguishing one from the other. In practical computations, this is easily accomplished by merely monitoring the Padé table when passing from one Padé approximant $P_K^{\pm}(z^{\pm 1})/Q_K^{\pm}(z^{\pm 1})$ to $P_{K+m}^{\pm}(z^{\pm 1})/Q_{K+m}^{\pm}(z^{\pm 1})\,(m = 1, 2, 3, ...)$. In so doing, as the order K of the FPT changes, we would observe that the parameters of some resonances are robustly stable, whereas the others exhibit great instability. Then the former resonances are identified as genuine and the latter as spurious. In practice, the first feature which is easily spotted in a long output table of spectral parameters from the FPT are literally hundreds of zeros or near-zeros in the column of the reconstructed amplitudes at certain frequencies. These will represent spurious, noise or noise-related resonances that, in turn, can confidently be dropped from the Padé output list, only if the corresponding pole-zero coincidences are observed at the same frequencies. Very feeble resonances cannot be discarded merely on the basis of smallness of their peak heights. For example, in medical diagnostics via MRS, certain true metabolites of diagnostic relevance could well have weak concentrations in the scanned tissue. Only in the case of a correlation between near zero-intensities and pole-zero near-confluences, could we identify/discard spurious resonances with fidelity.

There are many different procedures in various processors for attempting to improve signal-to-noise ratios (SNR). One of them also exists in the forward and root-reflected backward linear predictor (FB-LP) [9]. Here, the unphysical poles yielding diverging harmonics from the backward recursion are superficially forced to lie inside the unit circle via the so-called root reflection. Additionally, in order to partially improve SNR, averaging is performed for the predictions from the forward and root-reflected backward recursions. However, noticeable instabilities exist when attempting to distinguish signal from noise on the basis of near-equalities between poles generated by means of the forward and root-reflected backward LP expansion coefficients of the characteristic polynomial Q_K [8]. Such an obstacle is only partially mitigated by the said averaging technique from Ref. [9]. Nevertheless, both the non-averaged [8] and averaged [9] versions of this method, exhibit a common drawback of potentially missing weak genuine signal components when comparing the poles from the forward and root-reflected backward LP recursions. This is opposed to

the robust signal-noise separation in the fast Padé transform via the FPT$^{(\pm)}$, which exploits its additional degree of freedom via the denominator polynomial P_K, which is absent from all the variants of the LP model as well as from the auto-regressive (AR) processor. It is precisely this extra flexibility in the FPT, which sets the stage for the emergence of pole-zero confluences with the resulting null-amplitudes that subsequently enable the Froissart strategy to naturally filter out all redundancies via spurious or unphysical resonances from the reconstructed data.

Finally, we shall briefly address the problem of state survival probabilities of investigated systems in external fields by making a judicious combination of the Padé approximant and the Voigt-type function. As an example, we shall tackle a problem of surviving fractions of cells exposed to radiation doses D during various radiotherapeutic treatments. Here, a helpful link to MRS is possible by using the cell survival probabilities for assessing changes in concentrations of certain metabolites after radiotherapy as one of the methods in delineating the target volume for re-irradiated patients. Experimental data exist on integral intensities I of detected signals related to concentrations of several key metabolites (NAA, Cre, Cho,...) as a function of absorbed dose. Such observables for cyclic variations of metabolite concentrations in an irradiated tissue comprised of some J compartments could be modeled via $I = \sum_{j=1}^{J} A_j \sum_{k=1}^{K} S_{jk}(D)$, where A_j are the oscillation amplitudes. Here, $S_{jk}(D)$ are the cell surviving fractions for which e.g. the Voigt dose profile in the form of the Linear-Quadratic (LQ) model could be used $S_{jk} = \exp(-\alpha_{jk}D - \beta_{jk}D^2)$, or some other models might also be employed. Hereafter, for simplicity, we shall leave out the subscripts (j,k) and refer to the LQ model by $S_{\rm F}^{(\rm LQ)}(D) = \exp(-\alpha D - \beta D^2)$. Parameters α and β multiplying the linear (D) and quadratic (D^2) terms describe the direct cell kill and the cell repair pathways, respectively. The linear and quadratic terms dominate at low and high doses. Often, the LQ model compares reasonably well with experimental data at low and intermediate doses. However, this is not the case at higher doses for which experimental data behave like $\exp(-\lambda D)$ as opposed to the corresponding Gaussian asymptote $\exp(-\beta D^2)$ of the LQ model. Several attempts have previously been made to modify the incorrect high-dose behavior of the LQ model. This was done by introducing a Heaviside-type switching from the LQ model to the function $\exp(-\lambda D)$ at a certain transition dose $D_{\rm T}$ located within the high-dose region. To alleviate such a step function, we have made a Padé-type extension of the LQ model and, thus, proposed the Padé Linear Quadratic (PLQ) model [2, 3]. This was done by conceiving the argument $\alpha D + \beta D^2$ of the probability exponential in the LQ model as the first two expansion terms of a Maclaurin series. Such a series could be modeled by its Padé approximant as a ratio of two polynomials. Since the expansion coefficients of the series are themselves unknown, we have used the statistical Padé approximant. In so doing, the PLQ was constrained to simultaneously satisfy two conditions: (i) preservation of the LQ-prescribed effect $\alpha D + \beta D^2$ which becomes the numerator of the Padé approximant, and (ii) improvement of the incorrect high-dose limit of the LQ model by introduction of the denominator $1 + \gamma D$ in the argument of the exponential in the cell surviving probability. This gives the dose-effect curve in the PLQ model as $S_{\rm F}^{(\rm PLQ)}(D) = \exp[-(\alpha D + \beta D^2)/(1 + \gamma D)]$. Only one additional parameter $(\gamma > 0)$ is encountered in the PLQ relative to the LQ model. The quotient of two dose-dependent binomials in the PLQ model is justified by reference to the cell inactivation cross section, which is given by a ratio of the outgoing and incoming fluences per unit surface. The initial and final slope in the PLQ model are given by α/γ and β/γ, respectively. This implies that at high doses, the PLQ possesses the exponential fall-off $S_{\rm F}^{(\rm PLQ)}(D) \approx \exp(-\beta D/\gamma)$ in agreement with the observed pattern from experimental data. In the LQ model, the initial slope is α, but the high-dose limit of $S_{\rm F}^{(\rm LQ)}(D)$ keeps on bending following a Gaussian curve with no final slope. Parameters α, β and γ in the PLQ model are determined by a statistical perturbation-iteration procedure which reconstructs the input entries with machine accuracy for synthesized data in our benchmark computations. Detailed comparisons with many experimental data systematically revealed a clear out-performance of the LQ by the PLQ model. This is also evident from Fig. 4.

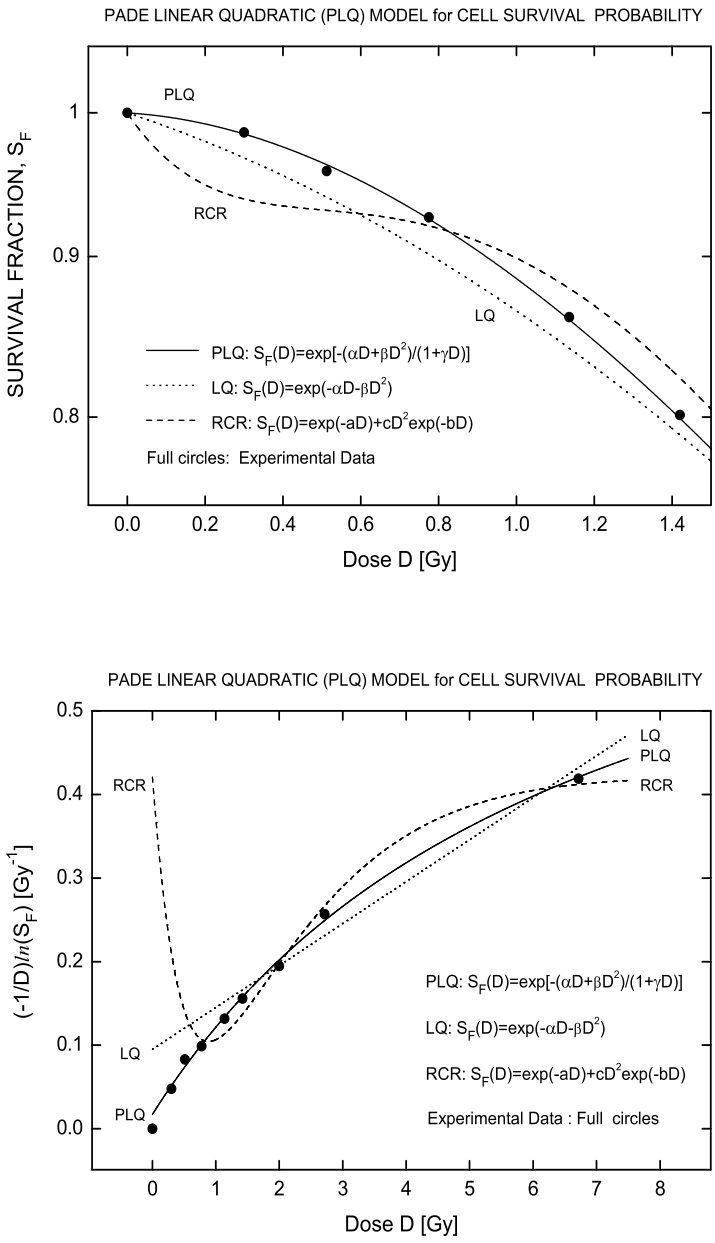

Figure 4: Measurements and radiobiological modelings of probability curves for cell survival fractions $S_{\rm F}(D)$ as a function of absorbed radiation dose D (top panel). In this graph, numbers on the ordinate are fractions of cells that survived an applied dose D expressed in units of gray (Gy). The bottom panel is the product of the reciprocal dose D^{-1} and the negative natural logarithm of $S_{\rm F}(D)$ as the ordinate versus D as the abscissa. In this so-called "full effect", or the Fe-plot, any departure of experimental data from a straight line indicates a failure of the related prediction $-(1/D)\ln(S_{\rm F}) = \alpha + \beta D$ by the Linear Quadratic (LQ) model. Experiment (solid circles): the mean clonogenic surviving fractions $S_{\rm F}(D)$ (top panel) and $-(1/D)\ln(S_{\rm F})$ (bottom panel) of the human small cell lung cancer line (U1690) irradiated by 190 kV X-ray [3, 4]. Theories: solid curve – PLQ (Padé Linear Quadratic) model, dotted curve – LQ model (the straight line $\alpha + \beta D$ on the bottom panel) and dashed curve – the model for Reparable Conditionally Repairable (RCR) damage [2, 3].

6 Conclusion

There are several important factors that can significantly influence the overall performance of parametric estimations in signal processing. The resolving power and convergence rate of all processors depend on certain obvious features of time signals, notably signal-to-noise ratio and the total acquisition time. Additionally, there are more subtle aspects of spectral analysis that can be of critical importance for accuracy and stability of all reconstructions for the sought response function of the given system exposed to external perturbations/excitations. Such are the key features of configurations of poles and zeros in the complex frequency plane, as well as the smallest distances among poles on the one hand and the zeros on the other. This becomes especially relevant when such distances are compared with the noise level, the density of signal poles and zeros, the pole-zero separations, the distance from the real frequency axis, the proximity of the unit circle and the smallest imaginary frequencies (line-widths) in the spectrum.

The most critical hurdle for spectral analysis is an unambiguous separation of genuine from spurious information in time signals. Using the fast Padé transform (FPT), we have shown that this exceedingly difficult and important problem can be solved via the powerful concept of exact signal-noise separation through Froissart doublets or pole-zero cancellations. This separation is unique to the FPT due to its defining polynomial quotient form P_K/Q_K of the frequency-dependent response function, which is the finite-rank approximation for the exact total Green function of the system. The true number K_G of genuine resonances, as the exact order or rank $K_{\rm ex}$ of the FPT with $K_G = K_{\rm ex}$ is not assumed or guessed, but rather it is explicitly reconstructed by reaching the constancy of P_K/Q_K when the polynomial degree K is systematically increased. By augmenting the 'running order' K above the plateau attained at $K = K_{\rm ex}$, the same values of P_K/Q_K are obtained via $P_{K_{\rm ex}+m}/Q_{K_{\rm ex}+m} = P_{K_{\rm ex}}/Q_{K_{\rm ex}}\,(m = 1, 2, ...)$. This can only be possible when for $K > K_{\rm ex}$ all the new poles and zeros coincide with each other, so that all the terms with these confluences are canceled from the canonical representation of P_K/Q_K. Furthermore, pole-zero confluences can also appear at any $K \leq K_{\rm ex}$. However, here also the corresponding amplitudes are invariably found to be equal to zero.

We have demonstrated that all zero-valued amplitudes and the associated pole-zero coincidences represent the unambiguous signatures of noise (or noise-like) i.e. non-physical information. The stated saturation effect, $P_{K_{\rm ex}+m}/Q_{K_{\rm ex}+m} = P_{K_{\rm ex}}/Q_{K_{\rm ex}}\,(m = 1, 2, ...)$, yielding the exact number $K_{\rm ex}$ of genuine resonances, occurs here in the course of the shape estimation i.e. without any quantification. In other words, even without retrieving the fundamental frequencies and amplitudes i.e. by doing solely non-parametric signal processing, the FPT can determine the true number $K_{\rm ex}$ of physical resonances. On the other hand, in its parametric mode of estimation, the FPT explicitly tackles the quantification problem and finds the exact solution of the underlying mathematically ill-posed and ill-conditioned harmonic inversion. Ill-posedness and ill-conditioning in spectral analysis refer to the fact that even very small perturbations and uncertainties (random errors, background noise and the likes) in the input time signals can cause huge errors in reconstructions, thus making the sought solution wildly unstable and, therefore, virtually non-existent. The FPT is shown to be safe-guarded against such ubiquitous perturbation instabilities by demonstrating that all the input parameters (complex-valued fundamental frequencies, amplitudes and their total number) in both noise-free and noise-corrupted time signals can be exactly reconstructed. This algorithmic robustness of the FPT is a direct consequence of the variational nature of the polynomial quotient representation for the Maclaurin series in powers of complex harmonic variable and time signal points as the expansion coefficients.

The joint distributions of poles and zeros in complex frequency planes are of primary relevance for noise recognition patterns. Argand plots are particularly helpful in the FPT for visualizing pole-zero cancellations of complex frequencies in the polar as well as the rectangular coordinates. Zero-valued spurious amplitudes for non-physical resonances as a function of chemical shift are also

displayed together with the positive values of the amplitudes for true resonances. The borderline of the unit circle in the complex plane of the harmonic variable is the natural accumulation or limiting region of noise or noise-related, spurious poles. This area of exceedingly small linewidths is always embedded in the Fourier spectra which, due to its linearity, imports noise as intact from the time to the frequency domain. In the non-linear FPT, noise and noise-like spurious spectral structures can be unmistakably identified through the accompanying pole-zero coincidences and the associated zero amplitudes. This is the basis of the Froissart-type noise suppression in the FPT. By this mechanism, spurious resonances of non-zero intensity regularly seen in Fourier spectra are absent from the corresponding Padé spectra by virtue of the annihilation of amplitudes of noisy resonances. This pattern explains the key noise-identification role of spectral zeros that the FPT treats on the same footing as the spectral poles. Genuine spectral zeros describe the valleys between the adjacent physical peaks whose positions are determined by locations of the true poles. By definition, the real-valued Fourier grid frequencies have exactly zero linewidths, thus lying precisely on the circumference unit circle in polar coordinates and, therefore, are entirely embedded in the noise-dominated borderline. Such a complete signal-noise inseparability is an extra obstacle to all quantifications based upon post-processing Fourier spectra. Quantification in the FPT is carried out autonomously without using the Fourier analysis. The FPT in rectangular frequency coordinates finds that all spurious poles in noiseless time signals are practically equidistant and aligned along nearly horizontal strings. When noise is present, distributions of these extraneous poles become unpredictable and chaotic even for very small random perturbations. However, in both noise-free and noise-corrupted cases, spurious resonances have zero amplitudes when plotted as a function of real frequencies or chemical shifts.

Detailed illustrations on these multifaceted pole-zero relationships are presented for the two equivalent variants of the fast Padé transform $\mathrm{FPT}^{(+)}$ and $\mathrm{FPT}^{(-)}$ that are initially defined inside and outside the unit circle, respectively, in the plane of the complex harmonic variable. In the $\mathrm{FPT}^{(-)}$ physical and non-physical resonances are inter-mixed outside the unit circles. Nevertheless, the denoising Froissart filter completely disentangles one from the other kinds of resonances according to the twofold signature via pole-zero coincidences and zero-valued amplitudes. On the other hand, in the $\mathrm{FPT}^{(+)}$, the true and spurious resonances are completely separated from each other in two disjoint portions of the complex frequency plane. This rigorous separation of genuine from spurious resonances represents a key feature for signal processing in biomedical applications and beyond.

It can be anticipated that the presently-described type of signal denoising through the Froissart filter within the exact Padé-based quantification methodology will have important and broad applications throughout various fields whose data analysis rely upon signal processing. The same FPT method can be used to quantify spectra that are not generated from time signals at all, such as those encountered in the standard time of flight experiments and many other types of measurements in which counts of events per channel are customarily recorded. For example, various types of Auger spectra that have been accumulated through measurements over the years in the literature of atomic, molecular and optical physics could advantageously be quantified using the present fast Padé transform. This would alleviate the need for the usual and ambiguous fitting techniques, since the FPT can yield the most accurate and unequivocal spectral parameters via the peak locations (transition energies), intensities and widths of the observed Auger lines alongside the reliable estimates of the possible satellite contributions.

Acknowledgment

This work was supported by the Swedish Cancer Society Research Fund, King Gustav the Fifth's Jubilee Foundation and the Nobel Medical University Research Fund.

References

[1] Günther H 2001 *NMR Spectroscopy*, 2nd Edn (John Willey & Sons: Chichester)

[2] Belkić Dž 2004 *Quantum-Mechanical Signal Processing and Spectral Analysis* (Institute of Physics Publishing: Bristol)

[3] Belkić K 2004 *Molecular Imaging through Magnetic Resonance for Clinical Oncology* (Cambridge International Science Publishing: Cambridge)

[4] Belkić Dž and Belkić K 2010 *Signal Processing in Magnetic Resonance Spectroscopy with Biomedical Applications* (Taylor & Francis: London)

[5] de Graff R A 2010 *In Vivo NMR Spectroscopy: Principles and Techniques* (John Willey & Sons: Sussex)

[6] Johnson M A, Jaudzems K and Wüthrich K 2010 *J. Mol. Biol.* **402** 619

[7] Mountford C E, Doran S, Lean C L and Russell P 2004 *Chem. Rev.* **104** 3667

[8] Delsuc M A, Ni F and Levy G C 1987 *J. Magn. Reson.* **73** 548

[9] Zhu G and Bax A 1992 *J. Magn. Reson.* **100** 202

[10] Alejos Ó, de Francisco C, Hernández P and Muñoz 1997 *Comput. Mater. Sci.* **7** 169

[11] Chen R, Ma G and Guo H 2000 *Chem. Phys. Lett.* **320** 567

[12] Levitina T V and Brändas E J 2001 *Comput. Chem.* **825** 55

[13] Taswell T 2000 *J. Comput. Appl. Math.* **121** 179

[14] Belkić Dž 2004 *Nucl. Instr. Meth. Phys. Res. A* **525** 366

[15] Belkić Dž and Belkić K 2006 *Phys. Med. Biol.* **51** 1049

[16] Belkić Dž and Belkić K 2009 *J. Math. Chem.* **45** 819

[17] Froissart M 1989 *CNRS, Recherche Cooperative sur Programme* N° 25, *Strasbourg*, Carmona J, Froissart M, Robinson D W and Ruelle D (Eds) **9** 1

[18] Gilevicz J and Kryakin Y 2003 *J. Comput. Appl. Math.* **153** 235

[19] Feifel R, Ueada K, de Fanis A, Okada K, Tanimoto S, Furuta T, Shindo H, Kitajima M, Tanaka H, Björneholm O, Karlsson L, Svensson S and Sorensen S L 2003 *Phys. Rev. A* **67** 032504

[20] Hatamoto T, Matsumoto, Liu X J, Ueada K, Hoshino M, Nakagawa K, Tanaka T, Tanaka H, Ehara M, Tamaki R and Nakatsuji H 2007 *J. Electr. Spectr. Rel. Phen.* **155** 54

[21] Takahashi O, Matsuyama K, Tabayashi K and Yamasaki K 2009 *J. Phys. B: At. Mol. Opt. Phys.* **42** 245102

[22] Press W H, Teukolsky S A, Vetterling W T and Flannery B P 1992 *Numerical Recipes in Fortran: The Art of Scientific Computing*, 2nd Edn (Cambridge University Press: Cambridge)

[23] Kreis R 1997 *J. Progr. Nucl. Magn. Spectr.* **31** 155

[24] Frahm J, Bruhn H, Gyngell M L, Merboldt K D, Hänicke W and Sauter R 1989 *Magn. Reson. Med.* **9** 79